Chromatographically Distinguishable Heme Insertion Isoforms of Human Hemopexin†

Marcia R. Mauk, Federico I. Rosell, and A. Grant Mauk*

Department of Biochemistry and Molecular Biology and the Centre for Blood Research, Life Sciences Centre, 2350 Health Sciences Mall, University of British Columbia, Vancouver, BC V6T 1Z3 Canada

Received September 5, 2007; Revised Manuscript Received October 5, 2007

ABSTRACT: Two spectroscopically distinct, non-interconverting forms of human hemopexin have been isolated by immobilized metal ion affinity chromatography and characterized spectroscopically. Form α (characterized by a bisignate Soret CD spectrum) and form *β* (Soret CD characterized by a positive Cotton effect) exhibit different spectroscopic responses to addition of Zn^{2+} or Cu^{2+}, yet both forms exhibit the same metal ion-induced decrease in T_m for the thermally induced release of the heme prosthetic group. Far UV−CD spectra indicate that the two isoforms possess essentially identical secondary structures, but their differential retention during metal ion affinity chromatography indicates slight differences in exposure of His residues on the protein surface. We propose that these observations result from the binding of heme in form *β* with an orientation that differs from the crystallographically observed binding orientation for rabbit hemopexin by rotation of the heme prosthetic group by 180° about the α−*γ meso*-carbon axis and from interaction of metal ions at two separate binding sites.

Hemopexin (Hx[1]; MW ∼ 58 000) is a type II acute phase reactant glycoprotein present in blood plasma. Circulating Hx is synthesized by the liver, but Hx is also reported to be synthesized by neural tissue (*1*). In addition to its primary function of scavenging heme released to the circulation by hemolysis or rhabdomyolysis (*2*−*4*), other roles reported for Hx include inhibition of phorbol-12-myristate-13-acetate-induced necrosis and adhesion of polymorphonuclear leukocytes (*5*−*7*). Removal of Hx from circulation is believed to be mediated by hepatic receptors, though the number of unique types of receptors as well as the cell types on which they occur remains unclear. Hepatic clearance of Hx that has lost terminal sialic acid residues is mediated by an asialoglycoprotein receptor while the Hx−heme complex is cleared by the action of a hemopexin-specific receptor (*8*). Receptor-mediated uptake of the Hx−heme complex leads either to encapsulation of the complex in endosomes where heme is released by acidification and apoHx returns to circulation (*9*) or in lysozomes where heme is released by proteolysis and no apo-Hx returns to circulation (*10*). At present, the factors that dictate the type of receptor that recognizes and thus determines the fate of the Hx−heme complex are not well understood.

Steric hindrance resulting from binding of heme to Hx inhibits oxidation of heme iron by hydroperoxides thereby preventing formation of highly oxidized iron species that have been implicated in the pathophysiology of cardiovascular disease and carcinogenesis (*11*). Heme binding to Hx exhibits contradictory characteristics in that heme binds with extremely high affinity (*12*, *13*) even though heme bound to Hx is relatively more exposed to solvent than is the case for heme bound to most heme proteins (*14*, *15*).

The crystal structure of the rabbit Hx−heme complex (*15*) shows that heme binds in a hydrophobic pocket with the A pyrrole vinyl (vinyl-2) and B pyrrole methyl group (3-methyl) fully exposed to solvent and with the heme propionate groups buried and involved in a variety of hydrogen bonding interactions. These interactions presumably account for the unusually high affinity of Hx for heme and for the extremely slow rate of heme release from the Hx−heme complex (*16*). Notably, however, one of the axial ligands to the heme iron is provided by His213, which is located in the flexible (linker) sequence that connects the N- and C-terminal domains of the protein. This region of the protein structure is characterized by relatively large thermal factors that are indicative of structural flexibility (*15*) that is presumably reflected in the behavior of the protein in solution.

Previously, we reported that the Soret CD spectrum of the human Hx−ferriheme complex exhibits a bisignate line shape that changes in response to the binding of either Zn^{2+} or Cu^{2+} (*17*). Prior to our report, however, others reported both bisignate (*18*) and non-bisignate (*19*) Soret CD spectra for this complex without comment. We now report the chromatographic separation of these two spectroscopic forms of this complex and the initial characterization of their properties. A structural rationale for these two forms is

† This work was supported by a Canadian Blood Services-Canadian Institute of Health Partnership Grant and a Canada Research Chair (A.G.M.). The spectropolarimeter and spectrophotometers were funded by grants from the Canadian Foundation for Innovation to the UBC Laboratory of Molecular Biophysics and the Centre for Blood Research and operated with support of the Michael Smith Foundation for Health Research.

* Author to whom correspondence should be addressed. Telephone: (604)822-3719. Fax: (604)822-6860. E-mail: mauk@interchange.ubc.ca.

[1] Abbreviations: Hx, hemopexin; heme, iron protoporphyrin IX; fwhm, full peak width at half maximum intensity; bisTris, 2-(bis(2-hydroxyethyl)amino)-2-(hydroxymethyl)propane-1,3-diol.

10.1021/bi701821a CCC: $37.00
Published on Web 11/29/2007

proposed in light of the model for the human Hx−heme complex reported previously (*5*).

METHODS AND MATERIALS

Sample Preparation. Human Hx was purified from plasma cryosupernate (Canadian Blood Services), and the Hx−ferriprotoporphyrin IX complex (Hx−heme) was prepared by addition of ferriheme (Frontier Scientific) as described previously (*17*, *20*, *21*). Following the final stage of purification involving elution over a nickel affinity resin (maximum load 20 mg of Hx−heme per 5 mL of HiTrap Chelating HP (GE Healthcare)), the chromatographic fractions were treated with EDTA (10 mM) to remove trace metal ions (*20*), and the fractions containing the Hx−heme complex were exchanged into bisTris buffers (pH 6.0 or 7.0, 50 mM bisTris (Sigma), 50 mM NaCl) by centrifugal ultrafiltration (AmiconUltra, 30 000 NMWL Millipore). A single broad band was observed for all Hx−heme fractions by SDS-PAGE under nonreducing conditions (*17*). With small amounts of protein loaded (<0.5 μg Hx per lane), two overlapping electrophoretic zones with centers that differ in apparent MW by ~1600 (PageRuler, Fermentas Life Sciences) can be distinguished within the broad electrophoretic band (as analyzed with a ChemiGenius^2 Bio Imaging System and associated software (GeneSap 6.05 for image acquisition and GeneTools 3.06 for data analysis), SynGene) that presumably reflect the heterogeneity of Hx carbohydrate composition (*17*, *22*−*24*).

Hx−ferriheme concentrations were determined on the basis of a molar absorptivity (280 nm) of 136 000 $M^{-1}cm^{-1}$ (*17*, *25*). Residue numbers are in accordance with the sequence alignment reported previously (cf. Figure 1 (*5*)). Solutions of $CuCl_2$ and $ZnCl_2$ were prepared from Titrisol standards (E. Merck).

Hx−ferroheme and Hx−ferroheme−CO samples were prepared in an anaerobic cuvette sealed with a rubber septum to facilitate purging of solutions with humidified CO or oxygen-free Ar gas and to allow addition of similarly deoxygenated sodium dithionite solutions with a Hamilton gastight syringe.

Electronic Absorption, CD, and MCD Spectroscopy. Electronic absorption spectra and thermal denaturation curves (15−95 °C) were collected as described previously (*20*) with Cary Model 6000i or 4000 spectrophotometers each equipped with a Peltier device. For high-resolution spectra, the slit width was reduced from 1 nm used for routine measurements to 0.5 nm, and the data interval was reduced from 0.25 to 0.05 nm. Thermodynamic parameters associated with heme release were calculated as previously described (*20*). Near UV and visible CD spectra were recorded with a Jasco Model J-810 spectropolarimeter (1 nm slit width and a 4 s averaging time and averaging at least three scans). Visible MCD spectra were obtained with a Jasco Model J-720 spectropolarimeter equipped with an Alpha Magnetics (Hayward, CA) electromagnet operating at a field strength of 1 T (calibrated by the method of Vickery (*26*)). Data collection parameters were the same as for CD spectra.

EPR Spectroscopy. A Bruker Spectrospin Model ESP-300e EPR spectrometer operated at X-band (~9.45 GHz) and fitted with an Oxford Instruments Model ESR900 continuous-flow liquid helium cryostat, gaussmeter, and Hewlett-Packard Model HP5352B microwave frequency counter was used for acquisition of EPR spectra. Spectra were obtained with modulation frequency and amplitude of 100 kHz and 10 G, respectively, and microwave power of 1, 1.25, or 5 mW at 4, 10, or 20 K. Rhombicity (V/Δ) and tetragonality (Δ/λ) were calculated as described by Palmer (*27*). The energy E_{yz} [$\equiv \Delta/3 + V/2$] (*28*) was calculated assuming a value of 400 cm^{-1} for the spin−orbit coupling constant, λ (*28*, *29*). Protein samples (230 μM) were prepared in bisTris buffer (50 mM, 50 mM NaCl, pH 6 or 7) with or without 10 equiv of Zn^{2+}.

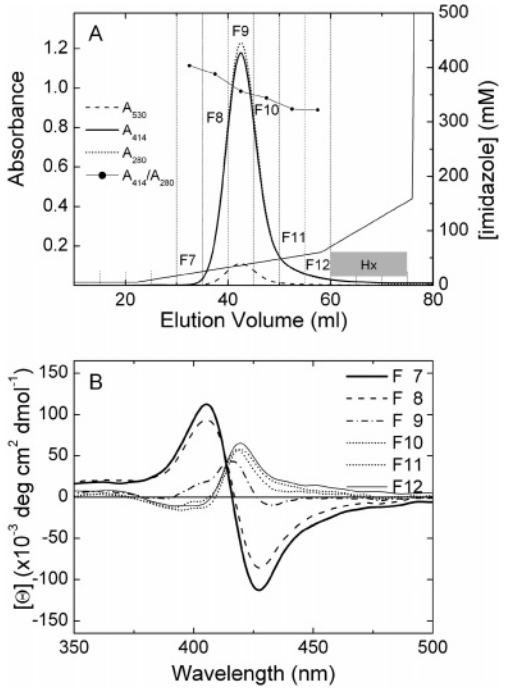

FIGURE 1: Chromatographic and CD spectral characterization of human Hx−heme. (A) Ni^{2+}-affinify chromatography of complex of human Hx and ferri-protoporphyrin IX. Fractionation of 6 mg of Hx−heme on Ni^{2+}-HiTrap chelating HP (5 mL) in sodium phosphate buffer (pH 7.4, 20 mM, 500 mM NaCl) with an imidazole gradient elution. Flow rate 5 mL/min, fraction size 5 mL, 22 °C. Absorbance at 280 nm (dotted line), 414 nm (solid line), 530 nm (dashed line). The horizontal gray bar indicates elution position of human Hx prior to addition of heme. The ratio of A_{414}/A_{280} of each fraction is indicated (connected solid circles), and these values correspond to the absorbance scale. (B) CD spectra of Ni^{2+}-affinity chromatography fractions of human Hx−heme. Fraction numbers are as indicated in part A. Spectra recorded at 25 °C in bisTris buffer (pH 7, 50 mM, 50 mM NaCl, 1 cm path length). Fraction 7 (bold line), 8 (dashed line), 9 (dot-dash line), 10 (dotted line), 11 (dotted line), and 12 (thin line) All samples contained 5−6 μM Hx−heme.

RESULTS

Isolation of Hx−Heme Complexes and Their CD Characterization. Chromatography on Ni^{2+}-immobilized affinity resin (Figure 1A) affords fractionation of the human Hx−heme complex into two forms with different Soret CD spectra (Figure 1B, Table 1). Spontaneous interconversion of these chromatographic forms has not been observed on the time scale of our studies or upon freezing and thawing. Optimal chromatographic separation of the two forms is achieved by loading amounts of protein that are substantially lower than the maximum resin capacity (Amersham technical bulletin (~12 mg protein/mL resin)). The observation that these two

Table 1: Soret-CD and Soret-MCD Spectroscopy Parameters of Human Hx−Heme Fractions Isolated by Ni^{2+}-Affinity Chromatography

		Hx−heme α		Hx−heme β	
		CD[a]	MCD[b]	CD	MCD
Hx–ferriheme	max	407.5 (100.3)[c]	406.4 (84.4)[d]	419.0 (55.7)	406.5 (81.0)
	min	428.2 (−88.0)	421.5 (−95.8)	396.0 (−12.3)	421.0 (−90.2)
Hx–ferriheme + 100 μM Zn^{2+}	max		406.3 (83.0)		406.4 (79.0)
	min		421.5 (−93.3)		421.0 (−90.6)
Hx–ferroheme	max	419.6 (90.5)			
	min	435.2 (−142.1)		422.0 (−24.9)	
Hx–ferroheme–CO	max	404.4 (5.2)			
		426.8 (3.6)			
	min	416.0 (−11.2)		421.2 (−19.5)	
		439.0 (−16.9)		428.2 (−19.2)	

[a] Spectra recorded in 20 mM sodium phosphate buffer, pH 7.2, 25 °C. [b] Recorded in 10 mM sodium phosphate buffer, pH 7.4, 20 °C, with a magnetic field of ∼1 T. [c] Band max/min wavelengths are cited with ellipticities in parentheses with units of 10^{-3} deg·cm²·dmol^{-1}. [d] $\Delta\epsilon/H$ values are cited in parentheses in units of M·cm·T^{-1}.

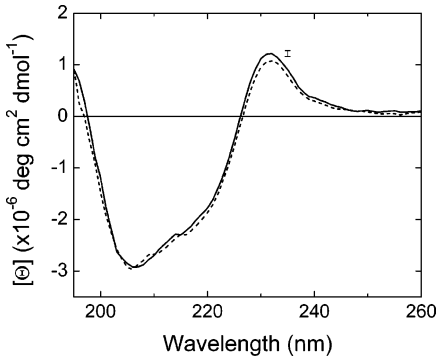

FIGURE 2: Far UV CD spectra of Hx−heme complex forms α and β. Spectra of form α (solid line) and form β (dashed line) (bisTris buffer, pH 7, 50 mM, 50 mM NaCl) are shown. The standard deviation of the reproducibility of the spectra at 231 nm is indicated by the error bar (placed at ∼235 nm for clarity).

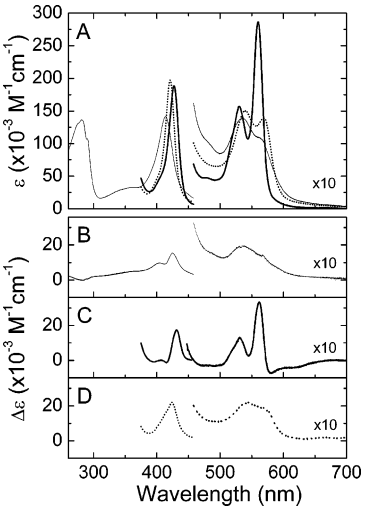

FIGURE 3: Comparison of the electronic absorption spectra of the Hx−ferriheme (thin line), Hx−ferroheme (bold line), and Hx−ferroheme−CO (dotted line) complexes (∼5 μM protein in 20 mM sodium phosphate buffer pH 7.2, 25 °C). (A) The spectra of form α are indicated by the line-types as defined above. (B−D) Form α-form β difference spectra for the three states of the Hx−heme complex studied here. Band widths and absorption maxima/wavelengths are summarized in Table 2.

forms of the Hx−heme complex are separated with an imidazole gradient suggests that the forms differ in the extent to which surface histidyl residues are exposed to solvent (*17*, *30*−*32*). Hx−heme is also well resolved from Hx under the chromatographic conditions (Figure 1A). The Hx−heme form eluting first (e.g., fractions 7 and 8) is designated as form α and exhibits a bisignate Soret region CD spectrum (λ_{max} = 405.5 nm, λ_{min} = 427.3 nm, and zero crossing at 416.1 nm (50 mM bisTris buffer (pH 7.0) 50 mM NaCl)). The Hx−heme form eluting second (fractions 10−12) is designated form β and exhibits a Soret CD spectrum with a single positive Cotton effect (λ_{max} = 419.5 nm) as its predominant feature. Fraction 9 contains a mixture of the two forms which were not resolved under the elution conditions of Figure 1A. The spectra were unchanged by lowering the pH to 6.0. The relative proportions of forms α and β produced upon addition of heme appears to vary with the blood donor.

Forms α and β exhibit nearly identical far-UV CD spectra (Figure 2). The positive ellipticity at 231 nm, which is more intense for the Hx−heme complex than for Hx alone and indicates the presence of the native Hx−heme structure (*20*, *21*, *33*−*35*), apparently arises from interactions between tryptophan side chains (*15*, *36*). This feature may be slightly more intense in the spectrum of form α than the spectrum of form β. The similarity of these two far-UV CD spectra provide evidence that the structures of forms α and β are nearly identical to each other and that the electronic spectra of the two forms should exhibit the same molar absorptivity at 280 nm. Nevertheless, the structural inequivalence of these forms is apparent from their differential elution during metal-affinity chelate chromatography and their markedly different Soret CD spectra. These differences are consistent with an altered arrangement of His residues at or near the surface of the protein and with different heme electronic environments, respectively.

Electronic Absorption Spectroscopy of the Hx−Ferriheme Complex. The Soret and visible absorption bands of both forms exhibit features typical of bis-histidine heme iron coordination (*19*, *37*, *38*) as expected from the structure of the rabbit Hx−heme complex (*15*) and a related model of the human Hx−heme complex (*5*). However, subtle differences in the spectra of the two forms of the protein are observed (Figure 3, Table 2). The spectra of the Hx−ferriheme, Hx−ferroheme, and Hx−ferroheme−CO derivatives of form α (Figure 3A) and the spectroscopic differences between forms α and β are also provided (Figures 3B−D). Form α of the Hx−ferriheme complex exhibits a Soret/$A_{280\ nm}$ ratio that is slightly greater than that of form β (Figures 1A and 3B and Table 2). The Soret λ_{max} of form α is also slightly (≤0.3 nm) red-shifted and is broader (∼1870 vs 1690

Table 2: Electronic Absorption Spectroscopy Characteristics of Human Hx−Heme Fractions Isolated by Ni^{2+}-Affinity Chromatography

	F8[a]	F11[a]
Hx−ferriheme[b]	413.8 (141.6; *1871*)[c]	413.7 (132.3; *1690*)
	534.2 (13.9)	535.4 (12.0)
Hx−ferriheme + 100 μM $ZnCl_2$	413.8 (138.3; *1842*)	413.8 (130.9; *1666*)
	534.9 (13.6)	534.8 (11.6)
Hx−ferroheme	427.4 (206.1; *1095*)	427.1 (169.5, *990*)
	530.5 (16.9)	529.7 (14.5)
	560.5 (31.4)	559.8 (25.7)
Hx−ferroheme−CO	420.8 (216.5; *1014*)	421.8 (178.0; *1001*)
	540.0 (15.4)	539.8 (14.7)
	568.0 (14.4)	570.4 (13.3)

[a] F8 and F11 refer to the elution position as defined in Figure 1. [b] Ferri-Hx spectra recorded in 10 mM sodium phosphate buffer, pH 7.4, 25 °C. [c] Soret and visible absorbance band peak wavelengths are as indicated. Absorptivities ($mM^{-1}\cdot cm^{-1}$) and Soret peak widths (cm^{-1} at fwhm) in italic type follow in parentheses. In all cases, a molar absorptivity of 130 000 $M^{-1}\cdot cm^{-1}$ is assumed at 280 nm.

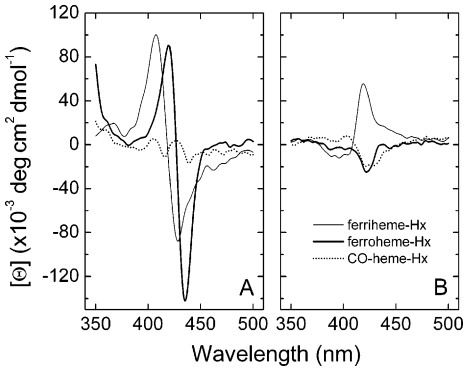

FIGURE 4: Comparison of the Soret CD spectra of the Hx−ferriheme (thin), Hx−ferroheme (bold), and Hx−ferroheme−CO (dotted) complexes (~5 μM protein in sodium phosphate buffer (pH 7.2, 20 mM, 25 °C). (A) Form α; (B) form β. Numerical results are summarized in Table 1.

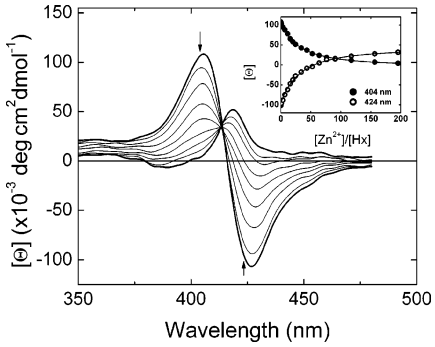

FIGURE 5: Dependence of the Soret CD spectrum of the Hx−heme complex form α on the addition of Zn^{2+} (sodium phosphate buffer (20 mM, pH 7.2, 25 °C)). The inset illustrates the dependence of ellipticity at 404 and 424 nm on [Zn^{2+}].

cm^{-1} fwhm) than that of form β. In contrast, the ratio of intensities of Soret to visible bands is lower for form α. From these observations, the differences in symmetry in heme environments (cf. Soret CD spectra) are also evident in the electronic spectra, indicating that while both forms α and β possess bis-histidine axial coordination to the heme iron their heme binding environments differ.

UV−Visible Absorption Characteristics of the Hx−Ferroheme Complex. The visible absorption spectra of the reduced and CO derivatives of form α (Figure 3A, Table 1) and difference spectra obtained by subtraction of the corresponding spectra of form β (Figure 3C,D) also indicate no major structural differences between the two forms of human Hx−heme but do reflect subtle differences in heme binding environment between the two forms of the protein. The α- and β-bands for the two forms of reduced human Hx−heme exhibit similar λ_{max} values and no evidence of splitting. Therefore, these two forms cannot explain the split α- and β-bands reported for rabbit Hx with deutero- (*19*) or occasionally for meso (*39*, *40*) ferroheme bound.

Inequivalent symmetry of the heme environments present in human Hx−ferriheme forms α and β that are evident from the Soret CD spectra are also evident in the CD spectra of the Hx−ferroheme complexes (Figure 4, Table 1). In the reduced state, form α retains its bisignate CD signature, intensifying and shifting to longer wavelengths as seen in the Soret absorbance. In contrast, the positive ellipticity that is characteristic of oxidized form β is replaced with a much smaller, negative ellipticity in the reduced state. Replacement of one of the axial histidine ligands (presumably His213 (*15*)) with CO eliminates most of the Soret CD in the spectra of both Hx−heme forms.

Interaction of Forms α and β with Metal Ions. Upon addition of Zn^{2+}, the CD spectrum of form α changes markedly from the bisignate profile shown in Figure 1B and 4A to a positive Cotton effect that resembles closely the CD spectrum of form β (Figure 5). The dependence of ellipticity at 404 and 424 nm on [Zn^{2+}] is shown in the inset. Although this spectroscopic conversion of form α can be reversed by addition of EDTA, addition of chelating agents to form β results in no spectroscopic response nor does addition of either Cu^{2+} or Zn^{2+}. In contrast to the Soret CD spectrum, the visible electronic spectrum of the two forms of the Hx−heme complex exhibit only minor changes in response to addition of Zn^{2+} (~25 cm^{-1} narrowing of the Soret band fwhm and reductions in molar absorptivity of ≤2% (Table 1)). Thus, in the presence of metal ions, the heme iron retains bis-histidine axial coordination with the subtle alterations in the electronic absorption spectra likely arising from electric field or polarity effects in the heme environment. However, strikingly, certain metal ions alter the asymmetry of the heme environment of form α, possibly converting it to a form β-like spatial geometry.

Our previous studies of the effects of metal ions on the human protein showed a wide influence on T_m and structural dynamics for Zn^{2+}, Cu^{2+}, Ni^{2+}, Co^{2+}, Mn^{2+}, Ca^{2+}, and Mg^{2+} (*5*, *17*, *20*, *21*). The present work refines and extends these observations by focusing on the specific effects of Zn^{2+} on the midpoint transition temperatures, T_m, and ΔH_m values for the transition associated with heme release from forms α and β that were determined on the basis of changes in

Soret intensity during thermal denaturation (sodium phosphate buffer, pH 7.4, 10 mM). These thermodynamic parameters (T_m values of 64.9 and 65.0 °C and ΔH_m of 102 and 113 kcal/mol for forms α and β, respectively) were within error[2] of values we reported previously for human Hx−ferriheme containing a mixture of forms α and β (*20*). The addition Zn^{2+} (to a concentration of 100 μM) had a similar effect on the release of heme from forms α and β (T_m of 58.4 and 58.2 °C with ΔH_m of 84 and 86 kcal/mol, respectively). On the basis of these observations, it is apparent that forms α and β exhibit very similar behavior when monitored in terms of the Soret absorbance and quite different behavior when monitored in terms of the Soret CD spectrum, emphasizing that the two techniques examine two different and possibly unrelated aspects of the response of the Hx−heme complex to Zn^{2+} binding.

In the thermal denaturation profiles, the slope of the change in Soret intensity at temperatures below the threshold for heme release is undoubtedly influenced by subtle protein structural dynamics similar to those observed in the absence of heme (*21*). For both forms, the fluctuations in Soret absorbance induced by increasing temperature were greater in the presence of Zn^{2+}. The influence of these conformational dynamics was evaluated by not including data collected at temperatures <37 °C in the fitting of the denaturation profile. Although this practice improved the statistical analysis of the resulting thermodynamic parameters, the interpretation of the results was unaffected.

MCD Spectroscopy. The Soret MCD spectra of Hx−heme forms (data not shown) are typical of six coordinate, low spin ferri-heme complexes (*19*, *41*). Only minor differences between the two forms were found (Table 1). Specifically, the MCD intensity is slightly greater, and the derivative-shaped spectrum in the Soret region is slightly broader for form α, in keeping with the visible absorbance of the two forms. The MCD spectra of both forms exhibited minimal change upon addition of Zn^{2+}.

EPR Spectroscopy. The identification of bis-histidine coordination in the rabbit Hx−heme crystal structure (*15*) and the similarity in visible spectra of the rabbit and human proteins (*2*, *42*, *43*) support the assignment of bis-histidine axial ligation in the human protein, To investigate the possibility of geometry changes in the histidine coordination as an explanation for the Soret and visible absorptivity differences between the two forms of human Hx−heme, EPR spectra of the two forms were obtained at pH 7.0 (Figure 6). Both forms α and β of the human Hx−heme complex exhibit predominantly low spin ($S = {}^1/_2$) ferric heme iron with $g_z = 2.90$, $g_y = 2.28$, $g_x = 1.55$ (i.e., rhombicity (V/Δ) of 0.61 and tetragonality (Δ/λ) of 3.27), consistent with bis-histidine axial coordination. These values are in excellent agreement with those reported previously for the human Hx−heme complex (*44*) and similar but not identical to values reported by others for both rabbit and human Hx−heme (*45*).

Comparison with EPR spectra reported for model systems (*46*, *47*) indicates that the spectra of forms α and β are consistent with parallel alignment of the planes of the axial His ligands and with a ~15° angle, ϕ, between these planes

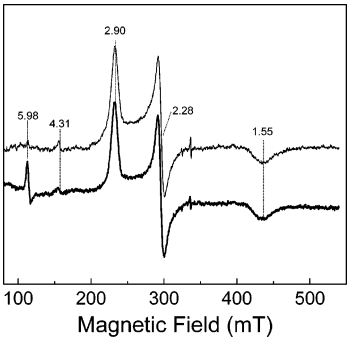

FIGURE 6: X-band EPR spectra (20 K) of Hx−ferriheme complex forms α (thin line) and β (bold line), pH 7.

and the nearest pyrrole N−Fe−N axis. However, differences in off-axis tilting of the axial ligands between the two forms cannot be ruled out because such perturbations are not reflected in the EPR spectra (*47*). The *g*-tensor values for forms α and β observed at pH 7 are nearly identical to those observed at pH 6.0 (data not shown). Comparison of the calculated value E_{yz} with those of proteins of known coordination (*28*) indicates that at low temperature (4−20 K) both forms have a protonated N1 position for the coordinated histidines at these pH values. The observation that addition of Zn^{2+} had no effect on the EPR spectrum of form α (data not shown) rules out the possibility (*17*) that Zn^{2+} binding induces an exchange of His213 for an adjacent His residue (e.g., His215) as a ligand to the heme iron.

DISCUSSION

We have recently shown that divalent metal ions influence the structural dynamics of Hx as well as stability of the Hx−heme complex (*17*, *20*, *21*). Plasma concentrations of divalent metal ions fluctuate during disease processes such as inflammation (*48*−*51*), and copper and zinc levels have recently been linked to structure and stability of the acute phase protein serum amyloid A (*52*). Thus, the influence of metal ion binding on the mechanism of heme binding to Hx may have a physiological role, and it may influence the proposed ability of Hx to provide protection against the oxidative toxicity of unbound heme.

Spectroscopic Results. Soret CD spectra of the human Hx−heme complex have been reported previously to possess either a single major positive feature at 418 nm with less intense transitions at shorter wavelengths (*19*) or to exhibit a bisignate spectrum with λ_{max} 404 nm, λ_{min} 424 nm (*18*). More recently, we reported conversion of the bisignate Soret CD line shape to a positive Cotton effect by addition of Cu^{2+} or Zn^{2+} (*17*). Our current results now make it apparent that previous studies were conducted with a mixture of two spectroscopically and chromatographically distinguishable forms of the protein.

Optical activity of heme proteins can arise from a variety of mechanisms unrelated to symmetry considerations at the coordinated heme iron. Considerable contributions to rotatory strength in the Soret CD can arise from out-of-plane twisting of vinyl groups, distortion from planarity of the heme, and dipole−dipole coupling between the heme and nearby amide groups or aromatic residues in addition to coupling with peptide $\pi-\pi^*$ transitions (*53*−*56*). The CD spectra of both the oxidized and reduced states of the two isolated forms of

[2] Reproducibility of $T_m = \pm 0.3$ °C and of $\Delta H_m = \pm 5$ kcal/mol.

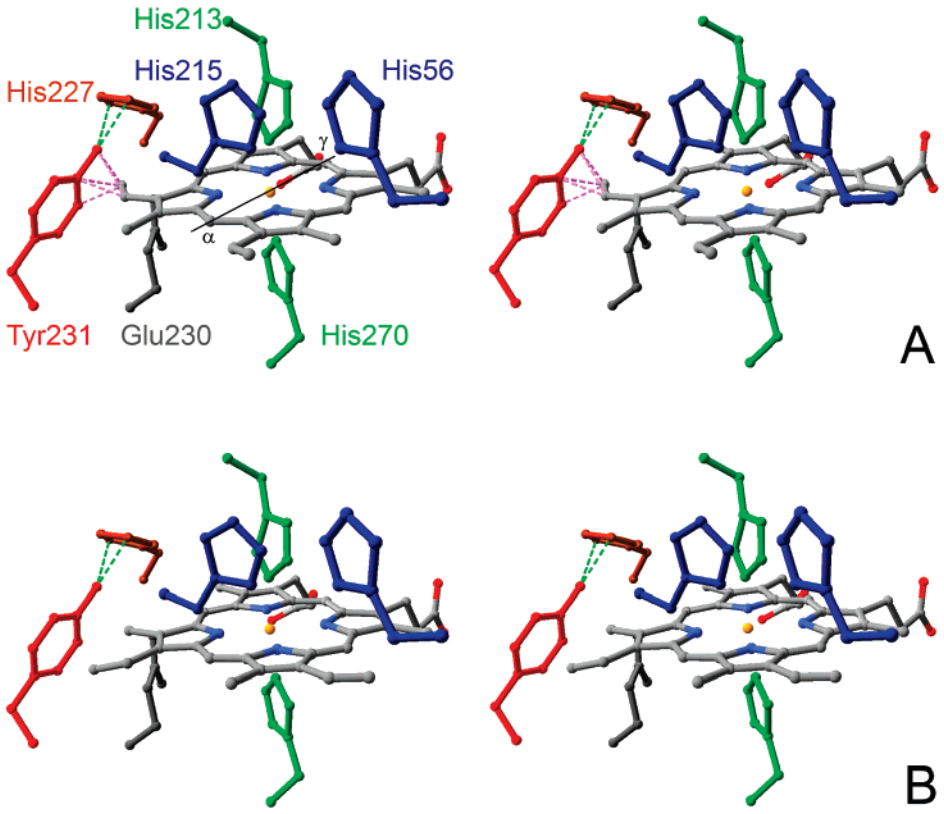

FIGURE 7: Stereodiagrams of the structures proposed for the human Hx−heme insertion isoforms. (A) Form α structure illustrating the heme orientation found in the structure reported for the rabbit Hx−heme complex (*15*). (B) Form *β* structure in which the heme is rotated 180° about the α−*γ* axis relative to the orientation shown in part A. Potential spatial conflicts (bond lengths <2 Å) between Tyr231 and the heme 4-vinyl group are depicted in magenta. His residues 56 and 215 comprising the bidentate metal ion binding Site I (*5*) are shown in blue, and the heme iron axial ligands (His213 and His270) are shown in green.

human Hx−heme show major differences. Form α is best described as bisignate in both oxidation states while the positive Cotton effect exhibited by form *β* is virtually eliminated upon reduction. The CO derivatives exhibit very weak CD spectra. This behavior suggests that conformational changes that accompany reduction of form *β* (but not α) and the binding of CO to the reduced form α significantly alter the symmetry in the heme vicinity possibly by elimination of strain on a vinyl group (form α) or alteration of interaction of heme with adjacent aromatic residues (form *β*). Thus form α may be viewed as constrained in an asymmetric heme environment until an axial His ligand (His 213) is replaced by CO. A possible explanation for these findings is that heme is inserted into Hx in one of two orientations that differ by a 180° rotation around the heme α−*γ* *meso*-carbon axis (Figure 7). The existence of rotational isomers demonstrated by NMR spectroscopy and crystallographic structure determination has been established for other heme proteins (*57*, *58*). Detection of these orientational isomers by CD but not by electronic absorption spectroscopy has been reported for sperm whale myoglobin (*59*, *60*) and hemoglobin (*61*). Therefore, the existence of subtle differences in the Soret/visible spectra of forms α and *β* and their differential responses to metal ions distinguish the human Hx−heme complex from other heme proteins that exhibit heme orientational disorder.

Proposed Structures for Forms α and β. The ability to separate chromatographically the two presumed heme orientational forms of the human Hx−heme complex is, at present, unique to this protein. This capability presumably results from two factors. First, Hx binds heme with extremely high affinity that most likely results from an exceptionally slow rate of dissociation of heme from the complex. Second, chromatographic resolution results from heme orientation-dependent structural differences that involve changes in surface histidyl residue accessibility presumably related to the histidine-rich linker sequence of human Hx. As a result, the properties of each form of the Hx−heme complex may be studied individually. As no interconversion of forms α and *β* has been observed in the present study, another consequence of an extremely slow rate of heme dissociation from the Hx−heme complex, we consider these two forms of the protein to be heme insertion isoforms rather than heme orientational isomers as observed for myoglobin, hemoglobin, and cytochrome b_5. With these latter proteins, initial binding of heme is followed by equilibration of the two orientational isomers to a final, thermodynamic equilibrium. In the case of the Hx−heme complex, such an equilibration process appears not to occur.

The experimental results reported here can be explained in terms of structural models we propose for forms α and *β* (Figure 7) on the basis of a structure for human Hx developed previously (*5*). In the model for form α (Figure 7A), heme is bound in the orientation observed in the crystallographically determined structure of the rabbit Hx−heme complex (*15*) while the model for form *β* (Figure 7B) involves heme binding after a 180° rotation about the heme α−*γ* *meso*-carbon axis. The key feature of these structures is the spatial arrangement around the 4-vinyl group, which in form α

conflicts with Tyr 231, giving rise to the bisignate Soret CD spectrum. The occurrence of Tyr231 at the C-terminal end of the linker region of human Hx (*5*) is notable because rat and rabbit Hx lack this additional Tyr residue in their linker sequences ((*18*, *62*−*64*), and the Hx−ferriheme complexes of these species do not exhibit a bisignate Soret CD spectrum (*18*).

The spectroscopic correlation of this structural feature is further supported by the failure of human Hx−heme complexes in which the 4-vinyl group is substituted (e.g., with H, C_2H_5, CH_2OH) to exhibit a bisignate Soret CD spectrum (*18*). We propose that the binding of Zn^{2+} or Cu^{2+} to a surface site (e.g., a site involving His56 and His215 (site I (*5*)) in the linker sequence) could cause rotation of Tyr231, perhaps through rearrangement of the linker main chain, that removes conflicts that generate the bisignate CD. The dependence of the Soret CD spectrum on metal ion concentration (Figure 6) is consistent with involvement of a low-affinity, possibly bidentate, binding site. A weak, bidentate interaction could explain the limited ability of Ni^{2+}, Mn^{2+}, or Co^{2+} to influence the Soret CD spectrum (*17*) insofar as these metal ions have more stringent coordination geometry requirements. Metal ion binding could also occur at a similar site in form β (Figure 7B), but it would have no spectroscopic consequence because Tyr231 is not adjacent to any heme substituents with heme bound in this orientation.

The similar thermodynamic stabilities of the two forms of the Hx−heme complex are also consistent with the proposed structural models (Figures 7A,B). Hx is unusual in that the residues that provide axial ligands to bound heme are not located in a structurally constrained region as indicated by dynamics calculations that show extremely low force constants for the coordinating residues (*65*). Thus, the environment around the buried heme propionate groups likely contributes extensively to the stability of heme binding. In the models for forms α and β, the 6- and 7-propionate groups occupy equivalent positions and should not be influenced differentially by metal ion binding at site I, for example. The effects of metal ions on heme release are, therefore, likely to arise from alteration in the extensive hydrogen-bonding network around the heme propionates (cf., Figure 3 (*15*)). Postulated metal ion binding site F (*5*) (residues Asp187, Glu 192, His 276) could participate in modulation of heme release by metal ions insofar as metal ion binding at this site would disrupt the H-bond between His276 and the 6-propionate of form α or the 7-propionate of form β, thereby facilitating heme release. This proposal is consistent with the ability of Zn^{2+} binding to lower T_m for both forms of the Hx−heme complex to the same extent. On the basis of these observations, it is reasonable to expect that the multiple metal ion binding sites with differing affinities in human Hx that were demonstrated by potentiometric titrations (*17*) may have specific functional roles.

Whether such heme insertion isoforms exist for other species of Hx is not clear. NMR studies of rabbit Hx that involved isotopically labeled hemin and cyanoheme adducts were interpreted to be consistent with but not clear evidence for heme orientational disorder in this protein (*16*). Similar NMR studies of the human and bovine proteins were prevented by poor signal-to-noise ratios that might be attributable to heterogeneity in glycosylation or to greater disorder in the linker sequence in which one of the axial ligands to the heme iron resides. The orientation of heme binding is reported to be identical in the crystal structures of the native and deglycosylated rabbit Hx−heme complexes (*15*). In time, additional insight concerning the occurrence of heme orientational isomerization in rabbit Hx may be provided by a more highly refined structure (B. Anderson and E.N. Baker, personal communication). Although the role of Hx glycosylation in heme binding is uncertain, NMR studies (*66*) are consistent with a decrease in mobility of some of the carbohydrate upon binding of mesoheme to rabbit Hx. Moreover, human Hx has an additional site of glycosylation at Asn217 (*5*, *62*, *63*) in the linker region that could, in principle, differentially favor heme binding in one of the orientations proposed in Figure 7 or that could tilt the plane of the heme prosthetic group with respect to the His-Fe-His axis.

Although no functional significance has been found for the rotational isomers of myoglobin (*67*, *68*), Walker and co-workers have observed a small difference in reduction potential for the major and minor heme orientation isomers of cytochrome b_5 (*69*). The relationship of the heme insertion isoforms to the interaction of the Hx−heme complex with receptors (*9*, *10*) and the ultimate fate of Hx remains to be evaluated. The possibility that Hx−heme function in heme scavenging as well as NO detoxification (*70*) could be regulated by an oxidation-state-dependent free energy difference between the two isoforms merits evaluation. Finally, it is also possible that our inability to crystallize the human Hx−heme complex in a form suitable for X-ray diffraction analysis may at least in part be a consequence of the occurrence of two heme insertion isoforms in the preparations of human Hx−heme that have been used for crystallization trials.

REFERENCES

1. Tolosano, E., Cutufia, M. A., Hirsch, E., Silengo, L., and Altruda, F. (1996) Specific expression in brain and liver driven by the hemopexin promoter in transgenic mice, *Biochem. Biophys. Res. Commun. 218*, 694−703.
2. Morgan, W. T., and Smith, A. (2001) Binding and transport of iron-porphyrins by hemopexin, *Adv. Inorg. Chem. 51*, 205−293.
3. Delanghe, J. R., and Langlois, M. R. (2001) Hemopexin: A review of biological aspects and the role in laboratory medicine, *Clin. Chim. Acta 312*, 13−23.
4. Tolosano, E., and Altruda, F. (2002) Hemopexin: Structure, function, and regulation, *DNA Cell Biol. 21*, 297−306.
5. Mauk, M. R., Rosell, F. I., and Mauk, A. G. (2007) Structural modelling of metal ion binding to human haemopexin, *Nat. Prod. Rep. 24*, 523−532.
6. Suzuki, K., Kato, H., Sakuma, Y., and Namiki, H. (2001) Hemopexins suppress phorbol ester-induced necrosis of polymorphonuclear leucocytes, *Cell Struct. Funct. 26*, 235−241.
7. Suzuki, K., Kobayashi, N., Doi, T., Hijikata, T., Machida, I., and Namiki, H. (2003) Inhibition of Mg^{2+}-dependent adhesion of polymorphonuclear leukocytes by serum hemopexin: Differences in divalent-cation dependency of cell adhesion in the presence and absence of serum, *Cell Struct. Funct. 28*, 243−253.
8. Smith, A. (1985) Intracellular distribution of haem after uptake by different receptors. Haem-haemopexin and haem-asialo-haemopexin, *Biochem. J. 231*, 663−669.
9. Smith, A., and Hunt, R. C. (1990) Hemopexin joins transferrin as representative members of a distinct class of receptor-mediated endocytic transport systems, *Eur. J. Cell Biol. 53*, 234−245.
10. Hvidberg, V., Maniecki, M. B., Jacobsen, C., Hojrup, P., Moller, H. J., and Moestrup, S. K. (2005) Identification of the receptor scavenging hemopexin-heme complexes, *Blood 106*, 2572−2579.
11. Timmins, G. S., Davies, M. J., Song, D. X., and Muller-Eberhard, U. (1995) EPR studies on the effects of complexation of heme

by hemopexin upon its reactions with organic peroxides, *Free Radic. Res. 23*, 559−569.
12. Hrkal, Z., Vodrazka, Z., and Kalousek, I. (1974) Transfer of heme from ferrihemoglobin and ferrihemoglobin isolated chains to hemopexin, *Eur. J. Biochem. 43*, 73−78.
13. Miller, Y. I., and Shaklai, N. (1999) Kinetics of hemin distribution in plasma reveals its role in lipoprotein oxidation, *Biochim. Biophys. Acta 1454*, 153−164.
14. Morgan, W. T., Sutor, R. P., and Müller-Eberhard, U. (1976) The aromatic and heme chromophores of rabbit hemopexin. Difference absorption and fluorescence spectra, *Biochim. Biophys. Acta 434*, 311−323.
15. Paoli, M., Anderson, B. F., Baker, H. M., Morgan, W. T., Smith, A., and Baker, E. N. (1999) Crystal structure of hemopexin reveals a novel high-affinity heme site formed between two beta-propeller domains, *Nat. Struct. Biol. 6*, 926−931.
16. Deeb, R. S., Müller-Eberhard, U., and Peyton, D. H. (1994) Proton NMR study of the heme complex of hemopexin, *Biochim. Biophys. Acta 1200*, 161−166.
17. Mauk, M. R., Rosell, F. I., Lelj-Garolla, B., Moore, G. R., and Mauk, A. G. (2005) Metal ion binding to human hemopexin, *Biochemistry 44*, 1864−1871.
18. Shipulina, N., Smith, A., and Morgan, W. T. (2000) Heme binding by hemopexin: Evidence for multiple modes of binding and functional implications, *J. Protein Chem. 19*, 239−248.
19. Morgan, W. T., and Vickery, L. E. (1978) Magnetic and natural circular dichroism of metalloporphyrin complexes of human and rabbit hemopexin, *J. Biol. Chem. 253*, 2940−2945.
20. Rosell, F. I., Mauk, M. R., and Mauk, A. G. (2005) pH- and metal ion-linked stability of the hemopexin-heme complex, *Biochemistry 44*, 1872−1879.
21. Rosell, F. I., Mauk, M. R., and Mauk, A. G. (2007) Effects of metal ion binding on structural dynamics of human hemopexin, *Biochemistry 46*, 9301−9309.
22. Kamboh, M. I., and Ferrell, R. E. (1987) Genetic studies of low-abundance human plasma proteins. VI. Polymorphism of hemopexin, *Am. J. Hum. Genet. 41*, 645−653.
23. Hrkal, Z., Kuzelova, K., Müller-Eberhard, U., and Stern, R. (1996) Hyaluronan-binding properties of human serum hemopexin, *FEBS Lett. 383*, 72−74.
24. Heide, K., Haupt, H., Stoeriko, K., and Schultze, H. E. (1964) On the heme-binding capacity of hemopexin, *Clin. Chim. Acta 10*, 460−469.
25. Seery, V. L., Hathaway, G., and Eberhard, U. M. (1972) Hemopexin of human and rabbit: Molecular weight and extinction coefficient, *Arch. Biochem. Biophys. 150*, 269−272.
26. Vickery, L. E. (1978) Spin states of heme proteins by magnetic circular dichroism, *Methods Enzymol. 54*, 284−302.
27. Palmer, G. (1985) The electron paramagnetic resonance of metalloproteins, *Biochem. Soc. Trans. 13*, 548−560.
28. Gadsby, P. M. A., and Thomson, A. J. (1990) Assignment of the axial ligands of ferric ion in low-spin hemoproteins by near-infrared magnetic circular dichroism and electron paramagnetic resonance spectroscopy, *J. Am. Chem. Soc. 112*, 5003−5011.
29. Walker, F. A. (1999) Magnetic spectroscopic (EPR, ESEEM, Mössbauer, MCD and NMR) studies of low-spin ferriheme centers and their corresponding heme proteins, *Coord. Chem. Rev. 185-186*, 471−534.
30. Hemdan, E. S., Zhao, Y. J., Sulkowski, E., and Porath, J. (1989) Surface topography of histidine residues: a facile probe by immobilized metal ion affinity chromatography, *Proc. Natl. Acad. Sci. U.S.A. 86*, 1811−1815.
31. Arnold, F. H. (1991) Metal-affinity separations: A new dimension in protein processing, *Bio/Technology 9*, 151−156.
32. Sulkowski, E. (1989) The saga of IMAC and MIT, *Bioessays 10*, 170−175.
33. Wu, M. L., and Morgan, W. T. (1994) Conformational analysis of hemopexin by Fourier-transform infrared and circular dichroism spectroscopy, *Proteins 20*, 185−190.
34. Morgan, W. T., and Muller-Eberhard, U. (1974) Modification of tryptophan residues of rabbit hemopexin by *N*-bromosuccinimide, *Enzyme 17*, 108−115.
35. Wu, M. L., and Morgan, W. T. (1993) Characterization of hemopexin and its interaction with heme by differential scanning calorimetry and circular dichroism, *Biochemistry 32*, 7216−7222.
36. Woody, R. W. (1994) Contributions of tryptophan side chains to the far-ultraviolet circular dichroism of proteins, *Eur. Biophys. J. 23*, 253−262.
37. Pajot, P., and Groudinsky, O. (1970) Molecular weight and quaternary structure of yeast L-lactate dehydrogenase (cytochrome b_2). 2. Revised heme extinction coefficients and minimal molecular weight, *Eur. J. Biochem. 12*, 158−164.
38. Chapman, S. K., White, S. A., and Reid, G. A. (1991) Flavocytochrome, b_2. *Adv. Inorg. Chem. 36*, 257−301.
39. Morgan, W. T., and Smith, A. (1984) Domain structure of rabbit hemopexin. Isolation and characterization of a heme-binding glycopeptide, *J. Biol. Chem. 259*, 12001−12006.
40. Shipulina, N., Hunt, R. C., Shaklai, N., and Smith, A. (1998) Coordination of nitric oxide by heme-hemopexin, *J. Protein Chem. 17*, 255−260.
41. Vickery, L., Nozawa, T., and Sauer, K. (1976) Magnetic circular dichroism studies of myoglobin complexes. Correlations with heme spin state and axial ligation, *J. Am. Chem. Soc. 98*, 343−350.
42. Hrkal, Z., and Müller-Eberhard, U. (1971) Partial characterization of the heme-binding serum glycoproteins rabbit and human hemopexin, *Biochemistry 10*, 1746−1750.
43. Müller-Eberhard, U., and Morgan, W. T. (1975) Porphyrin-binding proteins in serum, *Ann. N. Y. Acad. Sci. 244*, 624−650.
44. Aisen, P., Leibman, A., Harris, D. C., and Moss, T. (1974) Human hemopexin. Preparation and magnetic properties, *J. Biol. Chem. 249*, 6824−6827.
45. Bearden, A. J., Morgan, W. T., and Muller-Eberhard, U. (1974) Heme complexes of rabbit hemopexin, human hemopexin and human serum albumin: Electron spin resonance and Mössbauer spectroscopic studies, *Biochem. Biophys. Res. Commun. 61*, 265−272.
46. Soltis, S. M., and Strouse, C. E. (1988) Electronic structure of low-spin ferric porphyrins: Single crystal EPR evidence for pseudo-Jahn-Teller distortion in (tetraphenylporphinato)iron(III) bis(imidazole) cations, *J. Am. Chem. Soc. 110*, 2824−2829.
47. Walker, F. A. (2004) Models of the bis-histidine-ligated electron-transferring cytochromes. Comparative geometric and electronic structure of low-spin ferro- and ferrihemes, *Chem. Rev. 104*, 589−615.
48. Sobocinski, P. Z., Canterbury, W. J., Jr., Hauer, E. C., and Beall, F. A. (1979) Induction of hypozincemia and hepatic metallothionein synthesis in hypersensitivity reactions, *Proc. Soc. Exp. Biol. Med. 160*, 175−179.
49. Kushner, I. (1982) The phenomenon of the acute phase response, *Ann. N. Y. Acad. Sci. 389*, 39−48.
50. Conforti, A., Franco, L., Milanino, R., Totorizzo, A., and Velo, G. P. (1983) Copper metabolism during acute inflammation: Studies on liver and serum copper concentrations in normal and inflamed rats, *Br. J. Pharmacol. 79*, 45−52.
51. Oliva, J. C., Castell, M., Queralt, J., and Castellote, C. (1987) Effect of chronic inflammation on copper and zinc metabolism, *Rev. Esp. Fisiol. 43*, 25−31.
52. Wang, L., and Colon, W. (2007) Effect of zinc, copper, and calcium on the structure and stability of serum amyloid A, *Biochemistry 46*, 5562−5569.
53. Blauer, G., Sreerama, N., and Woody, R. W. (1993) Optical activity of hemoproteins in the Soret region. Circular dichroism of the heme undecapeptide of cytochrome *c* in aqueous solution, *Biochemistry 32*, 6674−6679.
54. Woody, R. (1978) Circular dichroism probes of hemoglobin structure, in *Biochemical and Clinical Aspects of Hemoglobin Abnormalities* (Caughey, W. S., Ed.) pp 279−298, Academic Press, New York.
55. Myer, Y. P. (1978) Circular dichroism spectroscopy of hemoproteins, *Methods Enzymol. 54*, 249−284.
56. Hsu, M. C., and Woody, R. W. (1971) The origin of the heme Cotton effects in myoglobin and hemoglobin, *J. Am. Chem. Soc. 93*, 3515−3525.
57. La Mar, G. N., Budd, D. L., Viscio, D. B., Smith, K. M., and Langry, K. C. (1978) Proton nuclear magnetic resonance characterization of heme disorder in hemoproteins, *Proc. Natl. Acad. Sci. U.S.A. 75*, 5755−5759.
58. Mathews, F. S. (1980) The orientation of the heme group in crystalline cytochrome, b_5. *Biochim. Biophys. Acta. 622*, 375−379.
59. Aojula, H. S., Wilson, M. T., and Drake, A. (1986) Characterization of haem disorder by circular dichroism, *Biochem. J. 237*, 613−616.
60. Aojula, H. S., Wilson, M. T., Moore, G. R., and Williamson, D. J. (1988) ^{1}H-NMR and CD studies of haem orientational disorder

in sperm-whale myoglobin and human haemoglobin, *Biochem. J. 250*, 853−858.
61. Kawamura-Konishi, Y., and Suzuki, H. (1985) Binding reaction of hemin to globin, *J. Biochem. (Tokyo) 98*, 1181−1190.
62. Takahashi, N., Takahashi, Y., and Putnam, F. W. (1985) Complete amino acid sequence of human hemopexin, the heme-binding protein of serum, *Proc. Natl. Acad. Sci. U.S.A. 82*, 72−77.
63. Morgan, W. T., Muster, P., Tatum, F., Kao, S. M., Alam, J., and Smith, A. (1993) Identification of the histidine residues of hemopexin that coordinate with heme-iron and of a receptor-binding region, *J. Biol. Chem. 268*, 6256−6262.
64. Nikkila, H., Gitlin, J. D., and Müller-Eberhard, U. (1991) Rat hemopexin. Molecular cloning, primary structural characterization, and analysis of gene expression, *Biochemistry 30*, 823−829.
65. Sacquin-Mora, S., and Lavery, R. (2006) Investigating the local flexibility of functional residues in hemoproteins, *Biophys. J. 90*, 2706−2717.
66. Cox, M. C., Le Brun, N., Thomson, A. J., Smith, A., Morgan, W. T., and Moore, G. R. (1995) MCD, EPR and NMR spectroscopic studies of rabbit hemopexin and its heme binding domain, *Biochim. Biophys. Acta 1253*, 215−223.
67. Aojula, H. S., Wilson, M. T., and Morrison, I. G. (1987) Functional consequences of haem orientational disorder in sperm-whale and yellow-fin-tuna myoglobins, *Biochem. J. 243*, 205−210.
68. Light, W. R., Rohlfs, R. J., Palmer, G., and Olson, J. S. (1987) Functional effects of heme orientational disorder in sperm whale myoglobin, *J. Biol. Chem. 262*, 46−52.
69. Walker, F. A., Emrick, D., Rivera, J. E., Hanquet, B. J., and Buttlaire, D. H. (1988) Effect of heme orientation on the reduction potential of cytochrome b_5, *J. Am. Chem. Soc. 110*, 6234−6240.
70. Fasano, M., Antonini, G., and Ascenzi, P. (2006) O_2-mediated oxidation of hemopexin-heme(II)-NO, *Biochem. Biophys. Res. Commun. 345*, 704−712.

BI701821A